# Design and Control of microscale Dual Locomotion Mode Multi-Functional Robots ( $\mu$ DMMFs)

Aaron C. Davis<sup>1</sup> and David J. Cappelleri<sup>1</sup>

Abstract—This paper presents the design and control of a novel microrobot that utilizes two distinct magnetic locomotion methods, a combination of rotating and gradient field control, for precise micro-object manipulation using multiple endeffectors. Rotating magnetic fields induce a tumbling locomotion mode to increase the movement speed and decrease issues associated with stiction and locomotion over rough surfaces. The gradient field control allows for precise manipulation using the end-effectors, which include a pointed tip for splitting groups of objects and a blunt end for pushing or capturing objects. The microrobot is fabricated using a two-photon polymerization 3D printer, allowing for the precise reproduction of complex geometries and designs. The potential applications of this technology in the medical field are discussed, highlighting the potential for in vitro cellular manipulation.

## I. INTRODUCTION

The field of microrobotics has been gaining increasing attention in recent years due to the wealth of potential biomedical applications for these small-scale microrobots. Wireless, untethered, microscale microrobots have the potential to perform tasks that are difficult or impossible for humans or traditional larger-scale microrobots, such as working in small, confined spaces and manipulating small, delicate objects [1]–[3].

Single-cell manipulation and surgery is a potential biological application where micro-robots specifically show promise. Micro-robots can be used to manipulate cells in vitro in a variety of ways, such as sorting, manipulating, or probing them in a controlled environment [4]-[6] as well as perforating them to inject drugs or other compounds [7]. The use of tumbling microrobots for biological applications is also very promising, as tumbling allows for increased movement speed and decreased problems with the complex, sticky terrain of the biological environment for both in vitro and in vivo applications [8]-[10]. Tumbling microrobots can be used to navigate through complex environments, such as the human body, with greater ease and efficiency. Additionally, tumbling microrobots can be used in applications where high-speed movement is required, such as rapidly scanning large areas or quickly traversing long distances.

One of the challenges in the field of mobile microrobotics is achieving precise control of the microrobot's movement for micromanipulation. A variety of control methods have been proposed, including the use of magnetic fields, piezoelectric actuation, and thermal actuation. Magnetic fields

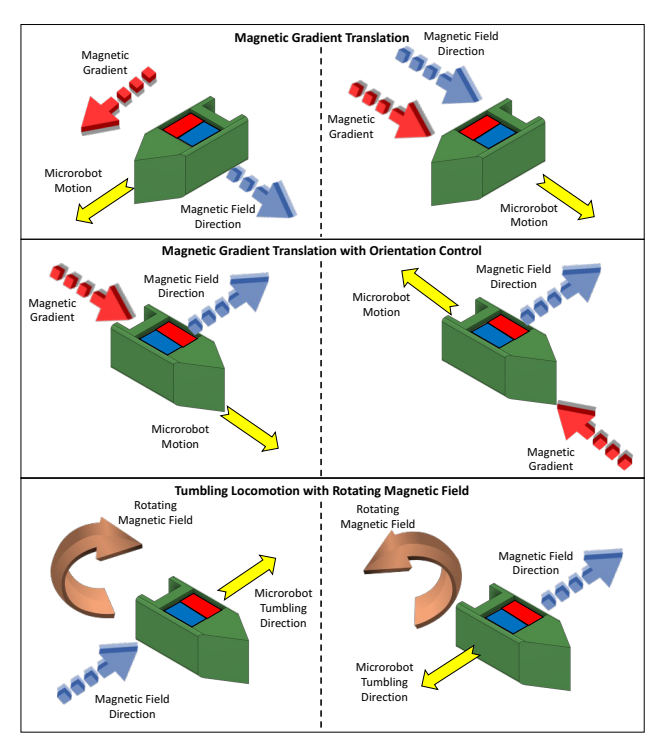


Fig. 1: Microscale Dual Locomotion Mode Multi-Functional Robots ( $\mu$ DMMFs): Magnetic mobile microrobots with distinct end-effectors can be controlled with gradient magnetic fields and rotating magnetic fields for multiple functions, such as single cell transport, micromanipulation, and single cell surgery.

have been particularly useful for controlling the movement of microrobots, as they can provide precise control even in the presence of obstacles or in confined spaces [11], [12]. Specific microrobot end-effectors can be developed for particular micromanipulation tasks. A wide range of end-effectors have been proposed and developed, including grippers, needles, tweezers, and other specialized tools. These end-effectors need to be able to manipulate small, delicate objects with high precision and dexterity [13]–[15]. However, these microrobots have only exhibited one such end-effector per microrobot, limiting the number of tasks that each can perform.

In this paper, we present a new multi-functional magnetic mobile microrobot design that combines the use of a rotating magnetic field for tumbling locomotion and a gradient magnetic field for precise movement control of the end-effectors. The microrobots are each equipped with two specialized end-effectors: a pointed tip for splitting groups of objects apart and a two types of blunt ends for either pushing an object or capturing and transporting objects (Fig. 1). This combination

<sup>\*</sup>This work was supported by the National Science Foundation under NSF IIS Award #: 1763689 and NSF CMMI Award #: 2018570

<sup>&</sup>lt;sup>1</sup>Aaron C. Davis and David J. Cappelleri are with the School of Mechanical Engineering, Purdue University, West Lafayette, IN 47907, USA. {davi1381,dcappell}@purdue.edu

of control methods and specialized end-effectors enables the microrobot to perform a wide range of micromanipulation tasks with high precision and dexterity. We will present the design and implementation of this approach, as well as experimental results demonstrating its effectiveness.

## II. DESIGN OVERVIEW

The  $\mu$ DMMFs were designed in two configurations. Each configuration has one end designed for separating clusters and fine manipulation of objects. On the other end, one configuration has an end-effector designed for pushing and local transport of a micro-objects, while the other has an end-effector designed for full capture and release of microobjects (Fig. 2). Captured objects can then be transported over obstacles or various terrains via tumbling. The entire  $\mu$ DMMF with the captured object can also be manually removed from the environment using tweezers and placed in another environment where the object can be released. The pushing and capture ends were both designed with open slits near the main body of the  $\mu$ DMMF. These slits are designed to enable directional fluid flow through the end-effector and increase the  $\mu$ DMMFs ability to stably push or capture and then release the object.

The  $\mu$ DMMFs are designed with a 250 $\mu$ m cubic enclosure with an opening on the top to hold NdFeB cube magnets. The control forces for magnetic microrobots are the magnetic force,  $\vec{F}_m$ , and the magnetic torque,  $\vec{T}_m$ , which are governed by the following equations with the magnetic moment of the microrobot,  $\vec{m}_r$ , and the applied magnetic field,  $\vec{B}$ :

$$\vec{F}_m = (\vec{m_r} \cdot \nabla)\vec{B}$$
$$\vec{T}_m = \vec{m_r} \times \vec{B}$$

The experimental system we are using generates gradients with magnitude up to  $\nabla \vec{B} = 1.5 \text{T/m}$  (See Sec.III for more details). This leaves  $m_r$  as the only variable we can change with our design. The magnetic moment of an object with magnetic remanence,  $B_r$ , and Volume, V, can be calculated using the equation:

$$m_r = \frac{B_r V}{\mu_o}$$

where  $\mu_o=1.25e^{-6}$  is the magnetic permeability of free space. As microrobots are specifically size limited, maximizing  $B_r$  is ideal. For this reason we have chosen a strong N50 grade NdFeB permanent magnet ( $B_r$ =1.6T) to be the magnetic portion of the  $\mu$ DMMFs. Due to the high strength of the permanent magnet body, large forces can be achieved with much smaller magnetic gradients. This is in contrast to the majority of microrobots which are controlled using rotating magnetic fields which exhibit much larger effective forces for a given field. A large control force decreases the effect which friction has on the movement of the microrobot and increases the microrobots ability to move large or sticky objects. Furthermore, the ability of the  $\mu$ DMMFs to split objects or cells which are attached together is increased. For the  $250\mu m$  NdFeB cube magnets used here, the magnetic moment comes out to be  $m_r = 19.9e - 6Am^2$ .

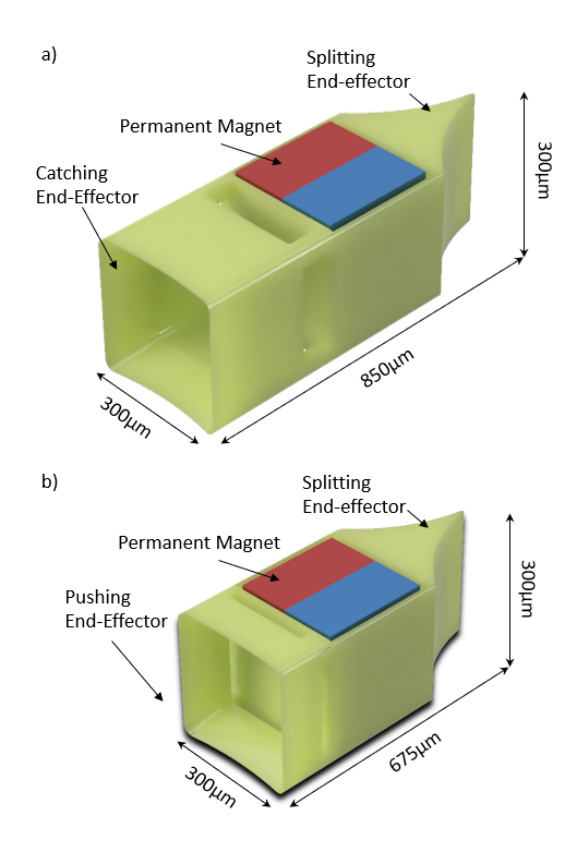


Fig. 2: Two  $\mu DMMF$  designs with different end-effectors. a)  $\mu DMMF$  with a capturing end-effector and a splitting end-effector. b)  $\mu DMMF$  with a pushing end-effector and a splitting end-effector. Both  $\mu DMMF$ s hold a 250 $\mu$ m cube magnet with the magnetic axis placed perpendicular to the acting direction for the end-effectors to ensure dual mode locomotion.

Thus, the expected maximum magnetic force applied to the  $\mu$ DMMF that can in turn be applied to the environment is approximately  $F_r = 30\mu N$ . This is much higher than the forces which can be exerted on microrobots using magnetic particles or nickel plating as is commonly done [1], [16], [17].

## III. MICROROBOT FABRICATION

These microrobots were fabricated using a Photonic Professional GT2 two photon 3D printer (Nanoscribe GMBH) with IP-S resin using a 25x objective on glass substrates with an indium tin oxide coating with standard slicing and laser settings provided by with the machine. While there has been work done that incorporates magnetic particles directly into the resin prior to printing, it is notoriously difficult to fully disperse the particles in the photoresin with a high enough concentration for reliable magnetic control and adequate printing performance. Therefore, we have decided to print a housing for microscale permanent magnet into the  $\mu$ DMMFs body and then assemble the magnet in the housing after printing. After the printing of the  $\mu$ DMMFs body is complete, a small bead of UV curable glue (Loctite 3926) is applied inside the enclosure that will house the magnet. The  $\mu$ DMMFs body is then removed from the substrate using tweezers and placed onto a 250 µm NdFeB cube magnet (SuperMagnetMan), which is held aligned with a bar magnet placed under an assembly substrate. The magnetic axis is

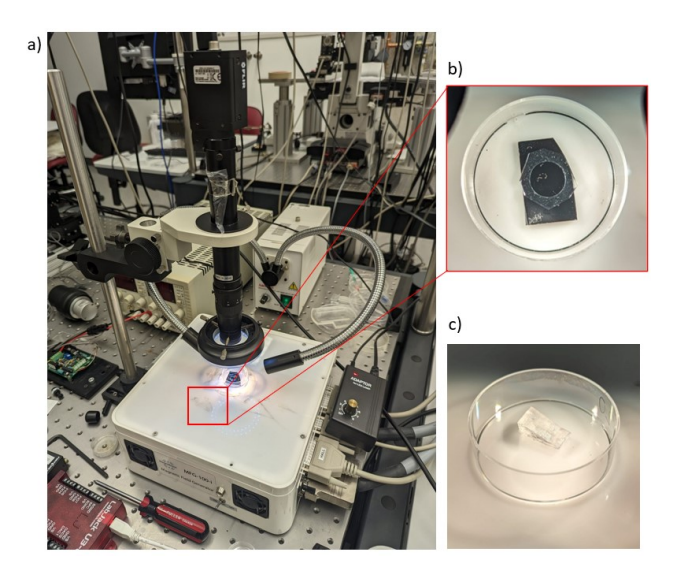


Fig. 3: Experimental setup. a) The MFG-100 system with a mounted microscope and ring-light. b) Substrate setup for locomotion and manipulation tests. A PDMS ring holds a well of silicone oil on top of a silicon wafer. c) Incline angle testing setup. The printed incline is glued to the bottom of a petri dish.

aligned to ensure dual mode locomotion with rotating an gradient magnetic fields in the manner required. Here, we align the poles of the magnet as shown in the schematic in Fig. 2.

#### IV. EXPERIMENTAL RESULTS

# A. Experimental Setup

The external magnetic fields use for driving the  $\mu DMMFs$  are generated using the MFG-100 system (Magnebotix AG) (Fig. 3). This system generates magnetic field up to 40mT and gradients up to 1.5T/m in a workspace which is 10mm in diameter. The system can independently control both the orientation of the field and direction of the gradient. Rotating fields with frequencies up to 2000Hz at 2mT and 100Hz at 8mT can also be generated.

Aligning the magnetic axis perpendicular to the two functional heads of the microrobot enables three important abilities. First, we can control and hold stable the vertical orientation of the microrobot enabling use of non-axially symmetric end-effectors during magnetic field gradient based translation. Second, we can independently control in-plane rotation and translation of the microrobot for object manipulation using the end-effectors. Third, we are able to tumble the microrobot sideways without compromising our end-effectors for faster and more consistent movement over the workspace.

Due to the relatively large stiction forces at the micro-scale of these  $\mu DMMFs$ , magnetic field gradient based control is only possible when the  $\mu DMMF$  is submerged in liquid. Common liquids used for this purpose are deionized water and silicone oil. In this instance the  $\mu DMMFs$  were placed on diced silicon wafers inside a PDMS ring and submerged in silicone oil Fig. 3b. The polished silicon substrate was utilized to further reduce friction and to help in imaging the transparent bodies of the microrobots by increasing contrast.

A hydrophobic coating could also be applied to reduce stiction even further [18] though this is not done here.

## B. Locomotion Experiments

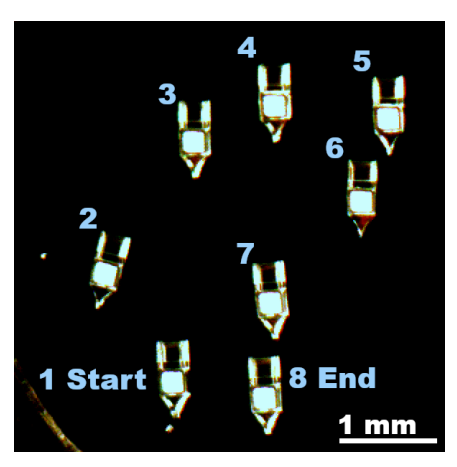
- 1) Mode 1: Translation Locomotion with Gradient Fields: Fig. 4a demonstrates effective control of a  $\mu$ DMMF aligned to a field including the ability to move in any direction without significant deviation in the orientation of the  $\mu$ DMMF. Furthermore, precise in-plane rotation is shown to be achieved in Fig. 4b. These images were taken using magnetic gradients up to 1.2T/m and a 6mT field strength.
- 2) Mode 2: Tumbling Locomotion with Rotating Magnetic Fields: Unlike the magnetic gradient locomotion mode, tumbling locomotion can be achieved on dry substrates, uneven or sticky terrain with significant slopes. Tumbling μDMMFs may even transition out of liquid environments when tumbling up a partially submerged slope. During our experiments in tumbling mode, the  $\mu$ DMMFs would often climb out of the PDMS ring to tumble across the dry petridish. As shown in Fig. 4c, we specifically demonstrated tumbling up and down a  $500\mu m$  tall  $18^{\circ}$  slope. Further incline slope testing was performed with a maximum climbable slope of  $20^{\circ}$  (Fig. 5) determined for this  $\mu$ DMMF design. The demonstrated tumbling was done using a 6mT field rotating at a frequency of 2Hz. The 18° slope was 3D-printed with the same material and procedure as the  $\mu$ DMMFs and then glued to the silicon substrate using UV curable glue. The other slopes (Fig. 3c) were printed using a Form 1+ stereolithography (SLA) 3D-Printer (Formlabs).

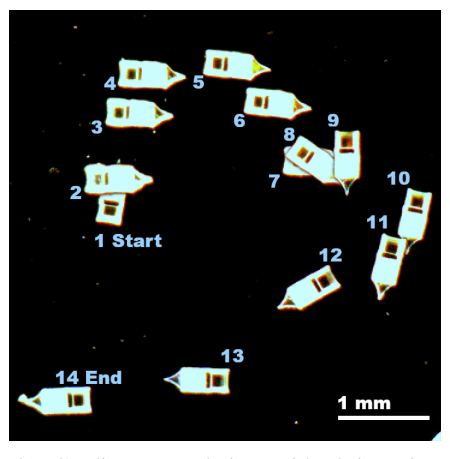
# C. Manipulation Experiments

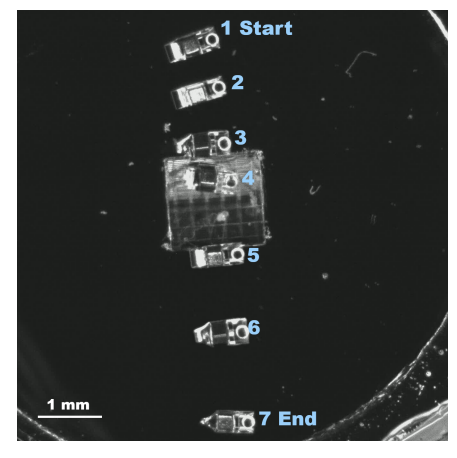
- 1) Object Capture: To demonstrate the use of the designed enclosed capture end-effector, we 3D-printed spherical beads with a  $200\mu m$  diameter, again using the same IP-S material as the  $\mu DMMF$  housings. In Fig. 4c and Fig. 6 the  $200\mu m$  bead is shown. Capture and release of the  $200\mu m$  beads are achieved using a 6mT magnetic field strength and magnetic gradients up to 1.2 mT/m. Capture of the beads required manipulating the target bead into a wall as there was not enough resistance to rolling to push the bead into the capturing end-effector. As seen in Fig. 6a at the third frame, the sphere starts to enter the end-effector. This partial capture is enough to maneuver the bead into the location against the wall to capture it completely. Releasing the beads works best with a backwards twisting motion as can be seen in steps 5-7 in Fig. 6b.
- 2) Micromanipulation: Reducing friction with the substrate through the methods described in Section IV enables precise control of the  $\mu$ DMMF end-effectors and precise object placement and micromanipulation. Fig. 7 shows the  $\mu$ DMMFs ability to manipulate 200 $\mu$ m beads into complex shapes. The limiting factor in creating these shapes is the constant drift of any beads which have already been placed.

# D. Manipulation Force Characterization Experiments

To measure the force the  $\mu DMMF$  can apply, cantilever beams were 3D-printed and glued to a silicon substrate







(a) Gradient Translation

(b) Gradient Translation with Orientation Control

(c) Tumbling Locomotion

Fig. 4: Locomotion Experiments: a) In gradient translation, the magnetic field orientation is held constant and a magnetic gradient is applied to the  $\mu DMMF$  to induce translation. Due to the orientation of the magnetic field, the pointed end-effector is held in a vertical position. b) By controlling the magnetic field orientation along withe magnetic field gradient, rotation is achieved alongside translation. c) Using an out-of-plane rotating magnetic field tumbling mode locomotion is used to climb a  $500\mu m$  tall  $18^{\circ}$  slope. In this image, the  $\mu DMMF$  is holding a captured  $200\mu m$  sphere object demonstrating effective and stable transport.

Incline Angle	Success (Y/N)	1 mm
5°	Υ	4 End 3 2 1 Start
10°	Υ	
15°	Υ	
20°	Υ	
25°	N	H

Fig. 5: Incline plane tumbling locomotion.  $\mu {\rm DMMFs}$  were able to climb slopes up to  $20^{\circ}.$ 

using the same UV curable glue mentioned above. The beam is 3D-printed with a large base and a fin which can be grasped by tweezers. This ensures that the beam can be picked up glued in the proper position on a substrate without damaging the fragile cantilever (Fig. 8a). The finetipped splitting end of the  $\mu$ DMMF was used to determine the manipulation force capabilities for the  $\mu$ DMMFs. The  $\mu$ DMMF is oriented perpendicular to the beam and a gradient field is applied. A notch near the tip of the beam matches the radius splitting end effector tip ensuring secure end-effector placement. Magnetic gradients ranging from 800mT/m to 1500mT/m with a 6mT orientation field were applied to push the  $\mu$ DMMFs into the beams and deflect them (Fig. 8b). From the images obtained from the experimental trials, the deflection data was extracted and used to calculate the manipulation force. Using the beam stiffness equations for a simply supported beam, the force applied by the  $\mu DMMF$ can be calculated as a function of the displacement  $\delta$  and

beam length L, height h, and base width b as:

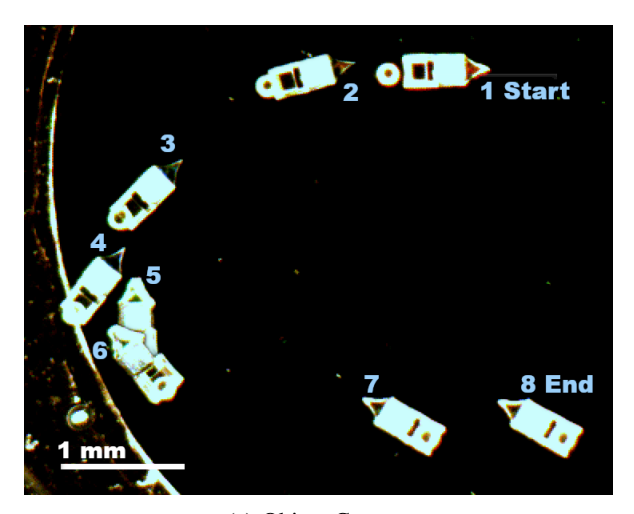
$$F = \frac{hb^3 \delta E}{4L^3}$$

The stiffness of 3D-printed IP-S is reported to be  $E=5.11 {\rm GPa}$ . A cantilever beam was 3D-printed with dimensions h=100 $\mu$ m, b=20 $\mu$ m, L=1500 $\mu$ m. If all the magnetic force was transferred to the beam, the deflection would be 91 $\mu$ m. The force deflection data is shown in Fig. 9. The deflection measured using the maximum magnetic gradient was 96 $\mu$ m which comes out to a value of 29 $\mu$ N. The calculated forces seem to follow the expected trend with a small offset due to the constant force of friction. The average loss due to friction is 4 $\mu$ N. This is smaller than expected, and is believed to be primarily due to two factors. The first is the efforts to reduce friction as mentioned in Section IV. The second is that these force measurements are done in such a way that static friction is not measured.

These results are particularly interesting in that they support the idea that the  $\mu DMMFs$  can be used for cellular surgery. In [19] it is shown that a force on the order of  $10^{-9}N$  is sufficient to puncture a HeLa cell. The  $29\mu N$  (order of  $10^{-5}N$ ) applied by the  $\mu DMMFs$  is 4 orders of magnitude larger. For single cell surgery applications, one must be also be careful not to damage the cells. The  $\mu DMMFs$  applied force can be controlled via the magnitude of the magnetic gradients applied. Thus, the  $\mu DMMF$  manipulation and puncture forces can be tuned for the particular cell type.

#### V. CONCLUSION

In this article we describe the fabrication and testing of  $\mu DMMFs$ , microrobots that have two methods of locomotion and end-effectors which fulfill several functions for micro-object manipulation and transport. These functions include local manipulation, capture, transport over terrain or across multiple dishes, and splitting of clusters. The problems explored in this research are of importance to the growing



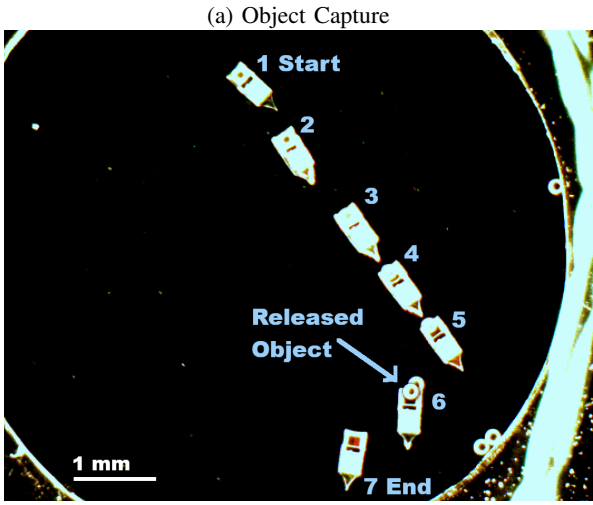


Fig. 6: Manipulation Experiments: Object Capture. (a) Using translation and orientation control, the capturing end-effector can manipulate and capture micro-objects. The objects are secure enough in the end-effector for transportation or removal from the environment along with the  $\mu$ DMMF. (b) Once brought to the desired location, the micro-object can be released.

(b) Object Release

field of microrobots for biomedical applications. While this work used 3D-printed micro-beads and other objects, cell manipulation, drug delivery, and micro-surgery are of great interest to the medical-microrobot community. This work can be further expanded upon to include more capture and release mechanisms. One way this can be done is by optimizing the shape of the microrobot to encourage flow of the submersing fluid. Additionally, new end-effectors can be explored. The pointed splitting tool can also be adjusted and utilized for cutting or puncturing. The fabrication approach used in this work can also be applied to a wide variety of active and passive end-effectors for cellular testing and manipulation. Future work will include investigating possible improvements to the existing designs and testing the locomotion and manipulation capabilities on and with living cells and tissues.

## **ACKNOWLEDGMENT**

We would like to thank the helpful faculty and staff at the Birck Nanotechnology Center as well as the Purdue College of Engineering.

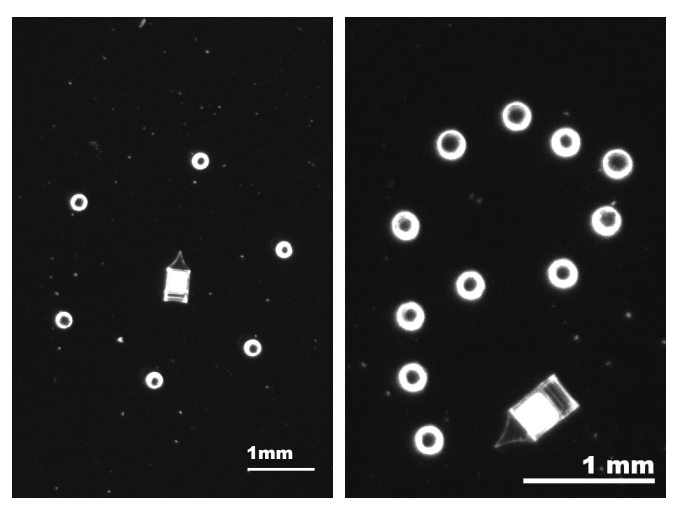
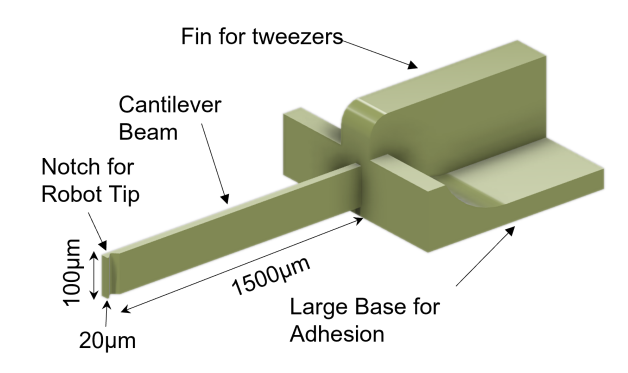
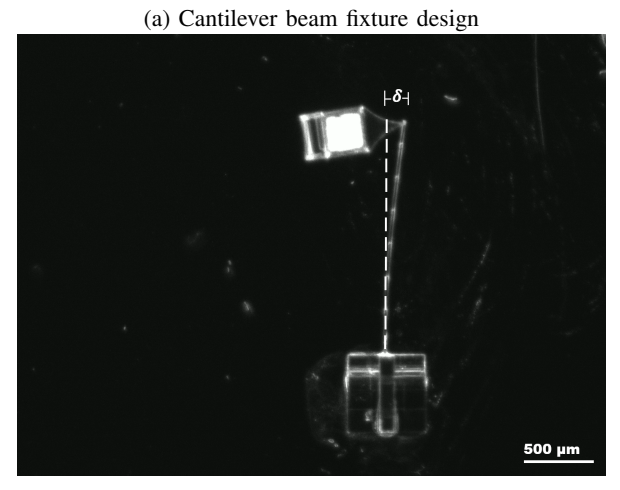


Fig. 7: Micromanipulation experiments: The pushing end-effector of the  $\mu$ DMMF was used to successfully arrange 250  $\mu$ m diameter microspheres into circular and P-shaped formations.





(b)  $\mu$ DMMF pushing on a cantilever beam

Fig. 8: Manipulation force characterization: a) 3D printed cantilever beam fixture schematic used to measure the force a microrobot can exert on objects. b) Using the fine-tipped splitting end of the  $\mu DMMF$  to deflect the cantilever to obtain deflection data needed to calculate the microrobot's manipulation force capability.

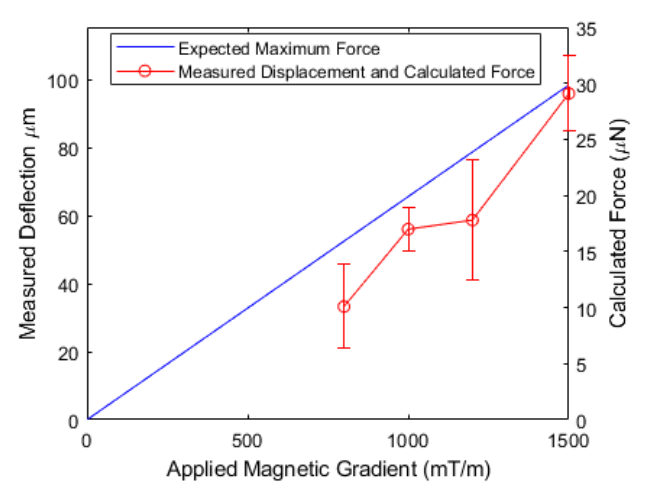


Fig. 9: The measured deflection of the cantilever beam under applied magnetic gradients. The axis on right hand side is scaled to show the calculated force based of the designed stiffness of the beam. The expected maximum force ignoring friction as discussed in Sec. II is also plotted to match the right hand side axis.

## REFERENCES

- [1] W. Jing, S. Chowdhury, M. Guix, et al., "A microforce-sensing mobile microrobot for automated micromanipulation tasks," *IEEE Transactions on Au*tomation Science and Engineering, vol. 16, pp. 518– 530, 2 2019, ISSN: 15455955.
- [2] G. Adam, S. Chowdhury, M. Guix, B. V. Johnson, C. Bi, and D. Cappelleri, "Towards functional mobile microrobotic systems," *Robotics 2019, Vol. 8, Page 69*, vol. 8, p. 69, 3 2019.
- [3] L. Feng, S. Liang, X. Zhou, *et al.*, "On-chip microfluid induced by oscillation of microrobot for noncontact cell transportation," *Applied Physics Letters*, vol. 111, 20 Nov. 2017, ISSN: 00036951.
- [4] B. Ahmad, T. Kawahara, T. Yasuda, and F. Arai, "Microrobotic platform for mechanical stimulation of swimming microorganism on a chip," in *IEEE/RSJ Int. Conf. on Intelligent Robots and Systems (IROS)*, Oct. 2014, pp. 4680–4685.
- [5] B. Ahmad, M. Gauthier, G. J. Laurent, and A. Bolopion, "Mobile microrobots for in vitro biomedical applications: A survey," *IEEE Transactions on Robotics*, pp. 1–18, 2021, ISSN: 1552-3098.
- [6] G. Adam, M. Hakim, L. Solorio, and D. J. Cappelleri, "Stiffness characterization and micromanipulation for biomedical applications using the vision-based forcesensing magnetic mobile microrobot," in 2020 International Conference on Manipulation, Automation and Robotics at Small Scales (MARSS), 2020, pp. 1–6.
- [7] A. Shakoor, W. Gao, L. Zhao, Z. Jiang, and D. Sun, "Advanced tools and methods for single-cell surgery," *Microsystems & Nanoengineering*, vol. 8, no. 1, p. 47, 2022.
- [8] C. Bi, M. Guix, B. V. Johnson, W. Jing, and D. J. Cappelleri, "Design of microscale magnetic tumbling robots for locomotion in multiple environments and

- complex terrains," *Micromachines*, vol. 9, pp. 1–17, 2 2018, ISSN: 2072666X.
- [9] L. Schwarz, D. D. Karnaushenko, F. Hebenstreit, R. Naumann, O. G. Schmidt, and M. Medina-Sánchez, "A rotating spiral micromotor for noninvasive zygote transfer," *Advanced Science*, vol. 2000843, pp. 1–14, 2020, ISSN: 21983844.
- [10] E. E. Niedert, C. Bi, G. Adam, et al., "A tumbling magnetic microrobot system for biomedical applications," *Micromachines*, vol. 11, p. 861, 9 Sep. 2020, ISSN: 2072-666X.
- [11] M. P. Kummer, J. J. Abbott, B. E. Kratochvil, R. Borer, A. Sengul, and B. J. Nelson, "Octomag: An electromagnetic system for 5-dof wireless micromanipulation," *IEEE Transactions on Robotics*, vol. 26, pp. 1006–1017, 6 Dec. 2010, ISSN: 15523098.
- [12] N. Ebrahimi, C. Bi, D. J. Cappelleri, *et al.*, "Magnetic actuation methods in bio/soft robotics," *Advanced Functional Materials*, vol. 31, no. 11, p. 2005 137, 2021.
- [13] Q. Zeb, C. Wang, S. Shafiq, and L. Liu, *An overview of single-cell isolation techniques*. Elsevier, Jan. 2019, pp. 101–135, ISBN: 9780128149195.
- [14] C. Yin, F. Wei, Z. Zhan, et al., "Untethered microgripper-the dexterous hand at microscale," *Biomedical Microdevices*, vol. 21, 4 Dec. 2019, ISSN: 15728781.
- [15] E. B. Steager, M. S. Sakar, C. Magee, M. Kennedy, A. Cowley, and V. Kumar, "Automated biomanipulation of single cells using magnetic microrobots," *International Journal of Robotics Research*, vol. 32, pp. 346–359, 3 Mar. 2013, ISSN: 02783649.
- [16] L. Tan and D. J. Cappelleri, "Design, fabrication, and characterization of a helical adaptive multi-material microrobot (hammr)," *IEEE Robotics and Automation Letters*, pp. 1–8, 2023, ISSN: 2377-3766.
- [17] T. Kawahara, M. Sugita, M. Hagiwara, *et al.*, "On-chip microrobot for investigating the response of aquatic microorganisms to mechanical stimulation," *Lab on a Chip*, vol. 13, pp. 1070–1078, 6 Mar. 2013, ISSN: 14730189.
- [18] M. Guix, J. Orozco, M. Garcia, et al., "Superhydrophobic alkanethiol-coated microsubmarines for effective removal of oil," ACS Nano, vol. 6, pp. 4445–4451, 5 May 2012, ISSN: 19360851.
- [19] W. Wang, Z. Wu, X. Lin, T. Si, and Q. He, "Gold-nanoshell-functionalized polymer nanoswimmer for photomechanical poration of single-cell membrane," *Journal of the American Chemical Society*, vol. 141, no. 16, pp. 6601–6608, 2019, PMID: 30943720.